nature structural & molecular biology

Association of condensin with chromosomes depends on DNA binding by its HEAT-repeat subunits

Ilaria Piazza[1–3], Anna Rutkowska[1,2], Alessandro Ori[2], Marta Walczak[1,2,5], Jutta Metz[1,2], Vicent Pelechano[4], Martin Beck[2] & Christian H Haering[1,2]

Condensin complexes have central roles in the three-dimensional organization of chromosomes during cell divisions, but how they interact with chromatin to promote chromosome segregation is largely unknown. Previous work has suggested that condensin, in addition to encircling chromatin fibers topologically within the ring-shaped structure formed by its SMC and kleisin subunits, contacts DNA directly. Here we describe the discovery of a binding domain for double-stranded DNA formed by the two HEAT-repeat subunits of the *Saccharomyces cerevisiae* condensin complex. From detailed mapping data of the interfaces between the HEAT-repeat and kleisin subunits, we generated condensin complexes that lack one of the HEAT-repeat subunits and consequently fail to associate with chromosomes in yeast and human cells. The finding that DNA binding by condensin's HEAT-repeat subunits stimulates the SMC ATPase activity suggests a multistep mechanism for the loading of condensin onto chromosomes.

The segregation of chromosomes during cell divisions depends on the action of multisubunit protein complexes named condensins. How condensins structure mitotic and meiotic chromosomes has, however, remained largely unknown[1–3]. Similarly little is known about the molecular mechanisms behind the increasing number of roles for condensin complexes during interphase[4]. A major reason for the lack of understanding of condensin function is that the interaction of the complex with its chromosome substrates has not yet been well defined.

Condensin complexes are composed of two structural maintenance of chromosomes (SMC) proteins (Smc2 and Smc4), which are characterized by ~45-nm-long antiparallel coiled coils, which separate 'hinge' dimerization domains from ATPase 'head' domains. Smc2 and Smc4 associate via their hinge domains and, after sandwiching two molecules of ATP in between each other, via their ATPase head domains[5]. A third subunit of the kleisin protein family[6] binds to the Smc2 head via its N-terminal helix-turn-helix (HTH) motif and to the Smc4 head via its C-terminal winged-helix domain (WHD)[7]. In addition to connecting the Smc2 and Smc4 heads, the kleisin subunit recruits two subunits that are predicted to be composed mostly of α-helical huntingtin, elongation factor 3, protein phosphatase 2A, Tor1 kinase (HEAT)-repeat motifs (**Fig. 1a**)[7,8]. In the budding yeast *S. cerevisiae*, the kleisin subunit Brn1 forms a single non-SMC subcomplex with the HEAT-repeat subunits Ycs4 and Ycg1. In human cells, the SMC2–SMC4 dimer associates with two distinct non-SMC subcomplexes. Condensin I contains the γ-kleisin CAP-H and the HEAT-repeat subunits CAP-D2 and CAP-G, and condensin II contains the β-kleisin CAP-H2 and the HEAT-repeat subunits CAP-D3 and CAP-G2 (ref. 9).

Condensin complexes isolated from *Xenopus laevis* egg extracts are able to bind to and change the topological and supercoiling states of circular plasmid DNAs in the presence of topoisomerases[10,11]. Individual SMC2–SMC4 or non-SMC subcomplexes, in contrast, bind to DNA only at very low salt conditions, fail to associate stably with chromatin in cell extracts and cannot promote changes in DNA topology or support the transformation into rod-shaped chromosomes of chromatin added to meiotic frog egg extracts[12]. Budding- and fission-yeast Smc2–Smc4 dimers, on the contrary, have been reported to bind to DNA and, in the case of the former, to induce the formation of knotted structures into plasmid DNA[13–15]. These findings are consistent with the suggestions that condensin's major DNA binding activity might be exerted by the Smc2–Smc4 subcomplex and that this activity is either enhanced[12] or diminished[15] by the non-SMC subcomplex.

An alternative hypothesis for how condensin complexes bind to DNA comes from the finding that DNA linearization or proteolytic opening of the tripartite ring structure formed by the Smc2, Smc4 and kleisin subunits releases the association between yeast condensin and circular minichromosomes *in vitro* and, in the case of the latter, between condensin and chromosomes *in vivo*[16]. Condensin rings might therefore encircle chromatin fibers topologically in a manner similar to that used by cohesin rings to entrap sister chromatids[17]. Interestingly, efficient release of condensin from minichromosomes required substantially higher salt concentrations than did release of cohesin[16], thus suggesting that condensin might make additional direct protein-chromatin contacts with DNA (as described above) or with histones[18,19].

[1]Cell Biology and Biophysics Unit, European Molecular Biology Laboratory (EMBL), Heidelberg, Germany. [2]Structural and Computational Biology Unit, EMBL, Heidelberg, Germany. [3]International PhD Programme, EMBL, Heidelberg, Germany. [4]Genome Biology Unit, EMBL, Heidelberg, Germany. [5]Present address: Max F. Perutz Laboratories, Vienna, Austria. Correspondence should be addressed to C.H.H. (christian.haering@embl.de).

Received 6 December 2013; accepted 24 April 2014; published online 18 May 2014; doi:10.1038/nsmb.2831

Although existing models propose defined tasks in DNA binding for the condensin SMC and kleisin components, the role of the two HEAT-repeat subunits has remained enigmatic. To gain insights into their contribution to condensin function, we biochemically and structurally characterized the two proteins as part of the condensin non-SMC subcomplex. We discovered that DNA binds to the *S. cerevisiae* non-SMC subcomplex and thereby activates the Smc2–Smc4 ATPases. Consistently with a role of the DNA-binding site in recruiting condensin to chromosomes, we found that condensin complexes that cannot assemble one of the HEAT-repeat subunits fail to associate with mitotic chromosomes in yeast and human cells. Our findings suggest that DNA binding by the non-SMC subcomplex and activation of the SMC ATPase constitute the first steps in the topological loading of condensin rings onto chromosomes.

RESULTS

The condensin non-SMC subcomplex binds DNA

To investigate the properties of the condensin non-SMC subcomplex, we coexpressed and purified from insect cells the *S. cerevisiae* kleisin subunit Brn1 and the HEAT-repeat subunits Ycg1 and Ycs4 (**Supplementary Fig. 1** and **Supplementary Table 1**). Coomassie staining of the peak elution fractions indicated that the three subunits formed a stoichiometric Brn1–Ycs4–Ycg1 subcomplex (**Fig. 1b**).

Because previous evidence suggested that condensin makes direct contacts with chromatin, we tested whether the non-SMC subcomplex might provide a platform for DNA binding. Although addition of the non-SMC complex did not notably affect the electrophoretic mobility of a 15-bp double-stranded DNA (dsDNA) substrate, it resulted in the formation of a slower-migrating species with 30-bp, 45-bp or 6.5-kb dsDNA (**Fig. 1c** and **Supplementary Fig. 2**). Fluorescence anisotropy assays to estimate the binding affinities between the Brn1–Ycs4–Ycg1 subcomplex and DNA in solution (**Fig. 1d**) revealed low-micromolar affinities for binding of the non-SMC subcomplex to the 30- and 45-bp dsDNA substrates ($K_d \approx 2$ μM).

The finding that the condensin non-SMC subcomplex efficiently binds to DNA was surprising, because the only predicted bona fide DNA-binding motifs present in the subcomplex are the HTH and WHD motifs at the N and C termini of the kleisin subunit[20]. In kleisin proteins, both motifs are, however, involved in binding to the SMC head domains[21–23]. To test whether these motifs were responsible for the observed DNA gel shift, we purified a subcomplex that contained a truncated version of Brn1 lacking both motifs ($Brn1_{\Delta NC}$; **Fig. 1e** and **Supplementary Fig. 1**). This $Brn1_{\Delta NC}$–Ycs4–Ycg1 complex bound the 30-bp dsDNA with an efficiency even slightly higher than that for the Brn1–Ycs4–Ycg1 subcomplex (**Fig. 1f** and **Supplementary Fig. 2**). We conclude that the non-SMC subcomplex binds to dsDNA substrates, most probably via its HEAT-repeat subunits.

Selective binding to double-stranded DNA helices

The Smc2–Smc4 dimer of condensin has previously been reported to bind to DNA via its hinge domain[24,25]. We therefore compared binding of the *S. cerevisiae* Smc2–Smc4 hinge and the non-SMC subcomplex to single-stranded (ssDNA) and dsDNA. The Brn1–Ycs4–Ycg1 subcomplex bound with low-micromolar affinity ($K_d \approx 2.0$ μM) to a 30-bp A-T dsDNA but not to a 30-base poly(T) ssDNA substrate (**Fig. 2a**). The Smc2–Smc4 hinge, in contrast, bound only the ssDNA substrate with appreciable affinity ($K_d \approx 0.3$ μM; **Supplementary Fig. 3**), consistently with the reported K_d and substrate specificity for the mouse Smc2–Smc4 hinge[25]. This experiment also suggests that the non-SMC subcomplex binds dsDNA with little or no DNA sequence specificity, because the affinities for two different 30-bp dsDNA substrates were very similar.

Because the kleisin subunits of fission-yeast and human condensin complexes have been reported to directly interact with tails of histone H2A and H2A.Z[18], we also tested binding of the *S. cerevisiae* non-SMC subcomplex to *in vitro*–reconstituted yeast nucleosomes[26] (**Supplementary Fig. 3**). Although we could not detect an electrophoretic mobility shift of the nucleosomal DNA, we noticed that

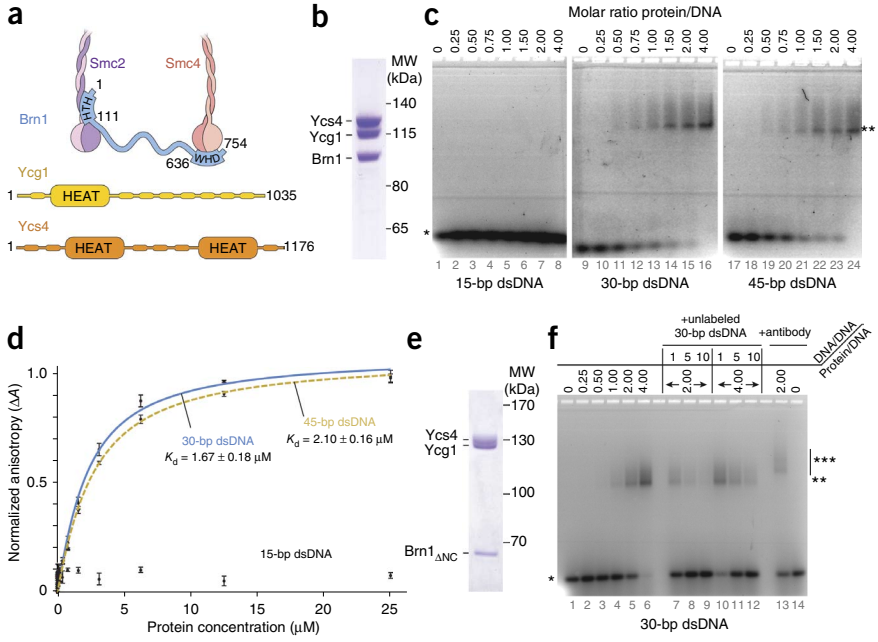

Figure 1 DNA binding by condensin non-SMC subcomplexes. (**a**) Schematic representation of the five condensin subunits labeled with the *S. cerevisiae* protein names. Amino acid residue numbers and positions of the helix-turn-helix (HTH) motif, winged-helix domain (WHD) and blocks of HEAT repeats are indicated. Small ovals indicate regions rich in α-helices. (**b**) Analysis of Brn1–Ycs4–Ycg1 after gel filtration by SDS-PAGE and Coomassie staining. MW, molecular weight. (**c**) Electrophoretic mobility shift assay (EMSA) of 15- to 45-bp dsDNA substrates, with 0.2 μM 6-carboxyfluorescein (6-FAM)–labeled dsDNA in the presence of 0.0–0.8 μM Brn1–Ycs4–Ycg1. Unbound (*) and slower-migrating species (**) are indicated. (**d**) Binding affinities of Brn1–Ycs4–Ycg1 to 15- to 45-bp 6-FAM–labeled dsDNA substrates, determined by measurement of fluorescence anisotropy changes (Δ*A*) upon addition of protein at the indicated concentrations. Dissociation constants (K_d) were calculated by fitting mean Δ*A* values for each protein concentration, assuming a single-site binding model. Points and error bars indicate mean and s.d., respectively, of $n = 3$ independent experiments. (**e**) Analysis of purified $Brn1_{\Delta C}$–Ycs4–Ycg1 as in **b**. The central region of Brn1 stains only weakly with Coomassie, as shown. (**f**) Electrophoretic mobility shift assay of a 30-bp dsDNA with $Brn1_{\Delta NC}$–Ycs4–Ycg1 as in **c** (lanes 1–6) after addition of unlabeled 30-bp competitor DNA (lanes 7–12) or an antibody against the hexahistidine (His_6) tag on Ycs4 (lanes 13–14). Unbound (*), slower-migrating (**) and antibody-supershifted (***) species are indicated. One representative experiment of $n = 3$ independent replicates is shown in **c** and **f**.

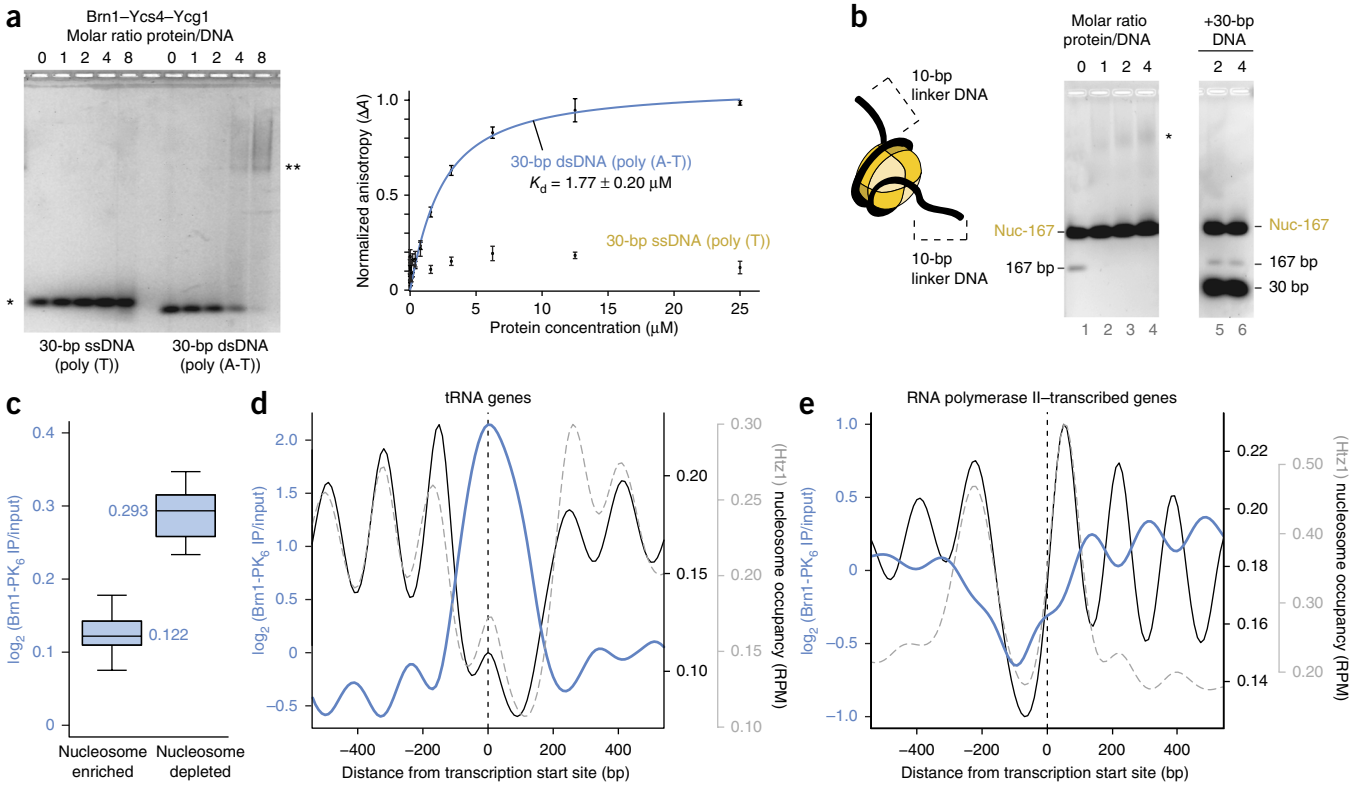

Figure 2 DNA and chromosome binding of the non-SMC subcomplex. (**a**) EMSA and fluorescence anisotropy binding assays of 6-FAM–labeled 30-bp dsDNA and ssDNA substrates with increasing Brn1–Ycs4–Ycg1 concentrations. Unbound (*) and slower-migrating species (**) are indicated. Points and error bars indicate mean and s.d., respectively, of $n = 3$ independent experiments. (**b**) EMSA of a 167-bp DNA assembled into a nucleosome (Nuc-167) and a small fraction (~2%) of free 167-bp DNA with increasing Brn1–Ycs4–Ycg1 concentrations before and after addition of a ten-fold excess of 30-bp competitor dsDNA. Upshifted free 167-bp DNA (*) is indicated. (**c**) Box plots showing assignment of Brn1 with six PK tags (Brn1-PK_6) ChIP-seq reads from yeast strain C3632 to nucleosome-enriched or nucleosome-depleted regions of the budding yeast genome; $P < 4 \times 10^{-9}$, Wilcoxon two-sided test. Horizontal lines define the median and boxes the 25th and 75th percentiles; whiskers represent the maximum and minimum values. $n = 16$ chromosomes. IP, immunoprecipitation. (**d**) Metagene analysis for the transcription start site (vertical dashed line) of all *S. cerevisiae* protein-coding genes. Condensin (blue line) expressed as enrichment over the input and average nucleosome (black line) or histone H2A.Z nucleosome (dashed gray line) occupancy expressed in reads per million (RPM), computed for each 10-bp bin and represented by smoothing splines. (**e**) Metagene analysis for all *S. cerevisiae* tRNA genes as in **d**. One representative experiment of $n = 3$ independent replicates is shown in **a** and **b**.

a small fraction of 167-bp DNA that had not been incorporated into nucleosomes was readily upshifted upon addition of the Brn1–Ycs4–Ycg1 subcomplex (**Fig. 2b**). The condensin non-SMC subcomplex therefore has a preference to bind free DNA over nucleosomal DNA.

The tendency for condensin's association with free rather than nucleosome-bound DNA became more apparent when we compared, by chromatin immunoprecipitation and massive parallel sequencing (ChIP-seq), the genome-wide distribution of budding-yeast condensin with that of nucleosomes in general[27] or histone H2A.Z-containing nucleosomes in particular[28] (**Fig. 2c** and **Supplementary Fig. 3**). The preference of condensin localization to nucleosome-free regions at transcription start sites was also evident at the promoters of tRNA genes (**Fig. 2d**) but not of RNA polymerase II–transcribed genes (**Fig. 2e**). Nevertheless, condensin binding patterns in the promoter-adjacent regions of both classes of genes appeared to correlate negatively with nucleosome binding patterns. Thus, binding of the *S. cerevisiae* non-SMC complex to free DNA helices *in vitro* reflects the preferred positioning of condensin complexes *in vivo*.

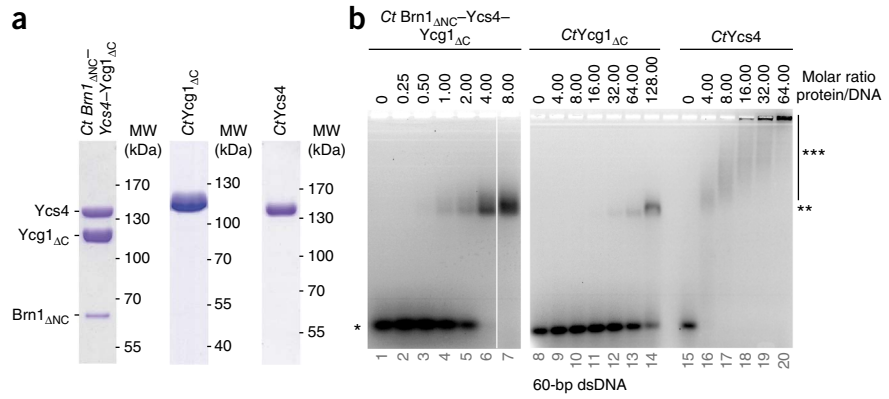

Figure 3 Both HEAT-repeat subunits are necessary for efficient dsDNA binding. (**a**) Purified *Ct* $Brn1_{\Delta NC}$–Ycs4–$Ycg1_{\Delta C}$ complex, *Ct*$Ycg1_{\Delta C}$ and *Ct*Ycs4, analyzed by SDS-PAGE and Coomassie staining. (**b**) EMSA of a 6-FAM–labeled 60-bp dsDNA at increasing concentrations of *Ct* $Brn1_{\Delta NC}$–Ycs4–$Ycg1_{\Delta C}$, *Ct*$Ycg1_{\Delta C}$ or *Ct*Ycs4. Unbound (*), *Ct* $Brn1_{\Delta NC}$–Ycs4–$Ycg1_{\Delta C}$ or *Ct*$Ycg1_{\Delta C}$-bound (**) and *Ct*Ycs4-bound complexes (***) are indicated. One representative experiment of $n = 3$ independent replicates is shown in **b**.

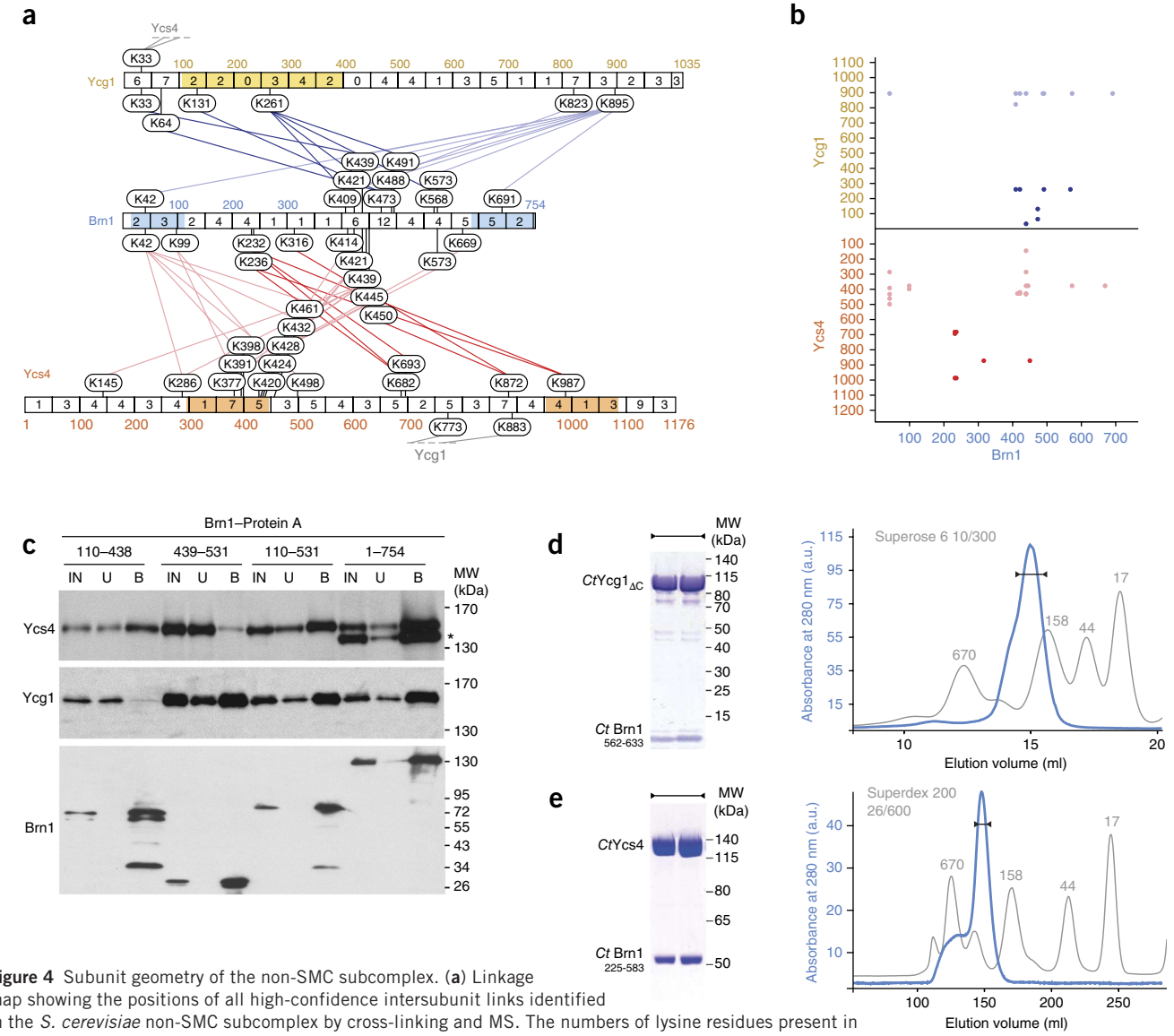

Figure 4 Subunit geometry of the non-SMC subcomplex. (**a**) Linkage map showing the positions of all high-confidence intersubunit links identified in the *S. cerevisiae* non-SMC subcomplex by cross-linking and MS. The numbers of lysine residues present in windows of 50 residues are indicated in squared boxes; HEAT-repeat, HTH and WHD motifs are indicated in color. Cross-links between the N or C termini of Ycg1 with Brn1 are indicated by dark- or light-blue lines, respectively; cross-links between the N or C termini of Ycs4 with Brn1 are indicated by pink or red lines, respectively. (**b**) Scatter-plot graph of the cross-links described in **a**. Residue numbers are indicated on the axes. (**c**) Western blotting against the PK_9 tag on Ycs4 or the HA_6 tag on Ycg1 in endogenous condensin subunits copurified with IgG beads. Samples are from *S. cerevisiae* expressing Protein A–fused fragments of the indicated Brn1 residues. IN, input; U, unbound; B, bound (10× concentrated compared to input) fractions. A band that results from binding of the anti-PK antibody by the full-length Brn1–Protein A is indicated by an asterisk. (**d**) SDS-PAGE and Coomassie staining of the *Ct* $Brn1_{562-633}$–$Ycg1_{\Delta C}$ complex after Ni-NTA chromatography, ion-exchange chromatography and gel-filtration chromatography (graph). (**e**) Purification of a stable *Ct* $Brn1_{225-583}$–Ycs4 complex as in **d**.

Efficient DNA binding requires both HEAT-repeat subunits

We next tested whether either of the two condensin HEAT-repeat subunits is capable of binding DNA individually. Because we could not purify sufficient amounts of the individual *S. cerevisiae* HEAT-repeat subunits, we expressed and purified the Ycs4 and Ycg1 subunits from the thermophilic yeast *Chaetomium thermophilum* (denoted by *Ct* prefix)[29] and compared their DNA binding activities to that of the *Ct* non-SMC subcomplex (**Fig. 3a** and **Supplementary Fig. 4**). In gel shift experiments, addition of the *Ct* $Brn1_{\Delta NC}$–Ycs4–$Ycg1_{\Delta C}$ subcomplex to a 60-bp dsDNA substrate produced a discrete slow-migrating band (**Fig. 3b**), similarly to the shift produced by the *S. cerevisiae* $Brn1_{\Delta NC}$–Ycs4–Ycg1 subcomplex (**Fig. 1f**). *Ct*Ycg1 or *Ct*Ycs4, in contrast, at high protein/DNA ratios, shifted either just a fraction of the dsDNA substrate into a discrete band ratio or into a diffuse streak of slower-migrating species that accumulated in the wells of the gel, respectively (**Fig. 3b**). These results suggest that the isolated condensin HEAT-repeat subunits are able to interact with DNA, albeit with considerably lower affinity than when they are part of the non-SMC subcomplex.

Subunit geometry of the condensin non-SMC subcomplex

To gain insights into the three-dimensional organization of the *S. cerevisiae* non-SMC subcomplex, we generated an interaction map of its subunits by using a cross-linking MS approach[30,31] (**Supplementary Fig. 5**). This identified 45 unique intersubunit and 48 intrasubunit cross-links (**Supplementary Tables 2** and **3**). Remarkably, out of the 45 intersubunit cross-links, only two connected

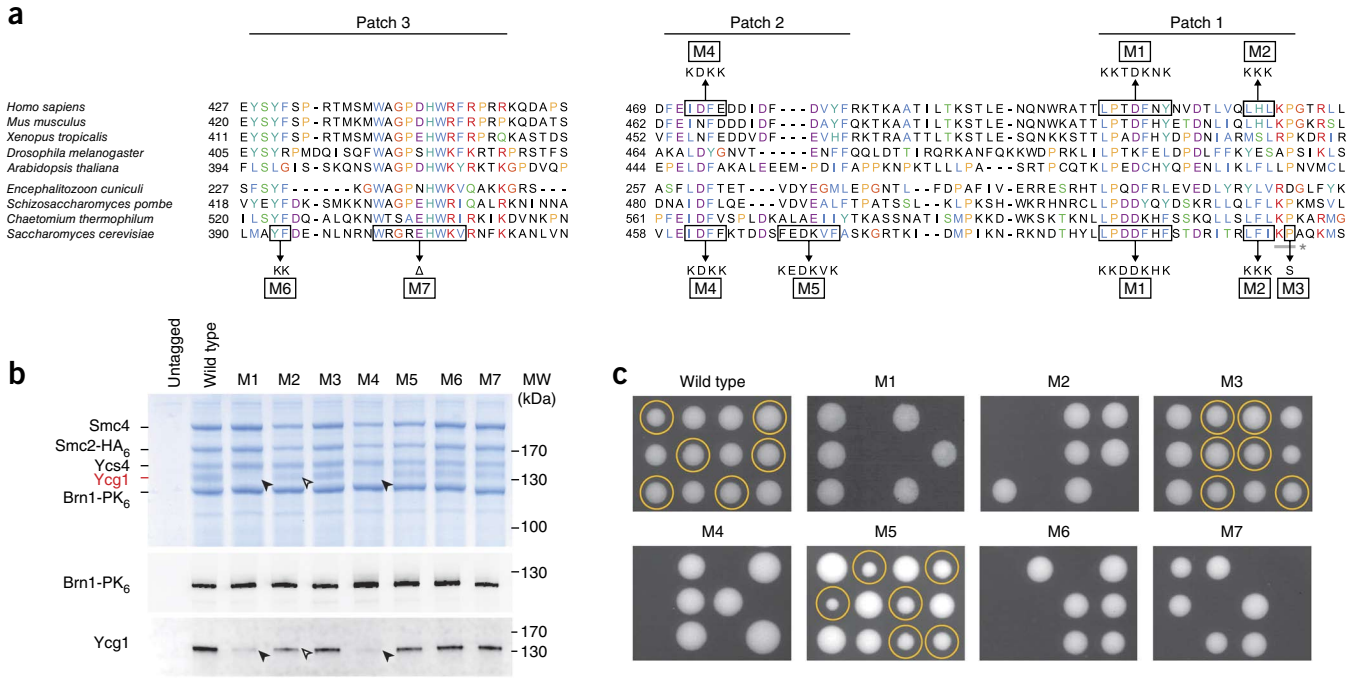

Figure 5 A conserved region within the Brn1 kleisin subunit for Ycg1 binding. (**a**) Multisequence alignment of the Ycg1-binding region of *S. cerevisiae* Brn1 with homologous γ-kleisins, identifying three patches of conserved amino acid residues. Boxed residues were mutated to the indicated sequences in mutants M1–M7. Two residues mutated in *brn1-60* are indicated by a gray bar and asterisk. (**b**) Coimmunoprecipitation of condensin subunits with the Brn1-PK$_6$ proteins from yeast cell extracts (strains C3632, C3665, C3651, C3641, C3635, C3658, C3649 and C3634), analyzed by Coomassie staining and western blotting with antibodies against Ycg1 or the PK epitope on Brn1. The Coomassie-stained bands were used in subsequent MS analyses. Loss or reduction of Ycg1 binding in mutants M1, M4 and M2 is indicated by closed or open arrowheads, respectively. (**c**) Tetrad dissection analysis of diploid cells from **b** at 30 °C on rich medium. Circles indicate kanamycin-resistant colonies linked to the wild-type or mutant *BRN1-PK$_6$* alleles. One representative experiment of $n = 3$ biological replicates is shown in **b** and **c**.

Ycs4 with Ycg1, whereas 27 or 16 links connected Brn1 with Ycs4 or Ycg1, respectively (**Fig. 4a**), thus suggesting that the HEAT-repeat subunits make little or no direct contact. This conclusion is consistent with the observations that the two HEAT-repeat subunits do not copurify (**Supplementary Fig. 6**), or do so only with very low efficiency[7], in the absence of the kleisin protein.

Notably, almost all cross-links with Ycg1 residues clustered within a small region of Brn1 (residues 409–573; **Fig. 4a**,**b**). To test whether this region forms a distinct binding domain for Ycg1, we expressed in budding yeast a series of Brn1 versions truncated either from the N or the C terminus and assayed which constructs bound endogenous Ycg1 (**Supplementary Fig. 6**). Ycg1 copurified only with Brn1 constructs that included the region between residues 439 and 531. Furthermore, this region of the kleisin subunit was sufficient for forming a stable complex with Ycg1 of *S. cerevisiae* (**Fig. 4c** and **Supplementary Fig. 6**) and *C. thermophilum* (**Fig. 4d**). Most cross-links with Ycs4 were located within a region N-terminal to the Ycg1-interacting domain (**Fig. 4a**,**b**). Although Ycs4 copurified from yeast extracts with Brn1 fragments that contained the region between residues 224 and 340, robust interaction required residues 110–438 (**Supplementary Fig. 6**). This region was sufficient for forming complexes with Ycs4 of *S. cerevisiae* (**Fig. 4c**) and *C. thermophilum* (**Fig. 4e**). We conclude that distinct binding domains exist within the central region of the condensin kleisin subunit for the recruitment of each HEAT-repeat subunit.

Active condensin complexes require both HEAT-repeat subunits

Because Ycg1 seems to bind only to a short region of Brn1, we reasoned that mutation of conserved hydrophobic residues clustered in two conserved patches within this region (patch 1 and patch 2) or in an additional patch just N terminal to it (patch 3; **Fig. 5a**) might prevent incorporation of Ycg1 into condensin complexes. We expressed mutant Brn1 versions from one of the two endogenous alleles in diploid *S. cerevisiae* cells (**Supplementary Fig. 7** and **Supplementary Table 4**) and assayed for copurification of Ycg1. Strikingly, Brn1 mutant M2 reduced binding and mutants M1 and M4 completely abolished binding to Ycg1 without affecting the association with the other three condensin subunits (**Fig. 5b** and **Supplementary Fig. 7**).

As would be expected if incorporation of Ycg1 into condensin complexes were essential for function, tetrad analysis demonstrated that Brn1 mutants M1, M2 and M4 failed to support growth at 30 °C in cells that also expressed Smc2 with six hemagglutinin tags (HA$_6$) (**Fig. 5c**). In the absence of a tag on Smc2, mutants M1 and M4 were able to sustain cell growth at 25 °C but not at 37 °C. We used these two mutants to test whether the observed growth defects were due to defects in chromosome segregation that result from condensin inactivation[32,33], by using live-cell microscopy to monitor partitioning of the fluorescently marked arm of chromosome V (ref. 16) in cells released from G1 phase at 37 °C (**Supplementary Fig. 7**). Remarkably, only 28% or 21% of Brn1-mutant M1 or M4 cells, respectively, successfully segregated the marked sister chromatids into opposite daughter cells within the time course of the experiment, compared to 75% of Brn1 wild-type cells. We conclude that yeast condensin complexes that are deficient in recruiting Ycg1 are unable to support proper chromosome segregation and cell division. Interestingly, mutations within patch 3 abolished condensin function without notably affecting Ycg1 or Ycs4 binding (**Fig. 5b**,**c**), thus suggesting that this patch has an essential function other than recruiting the HEAT-repeat subunits.

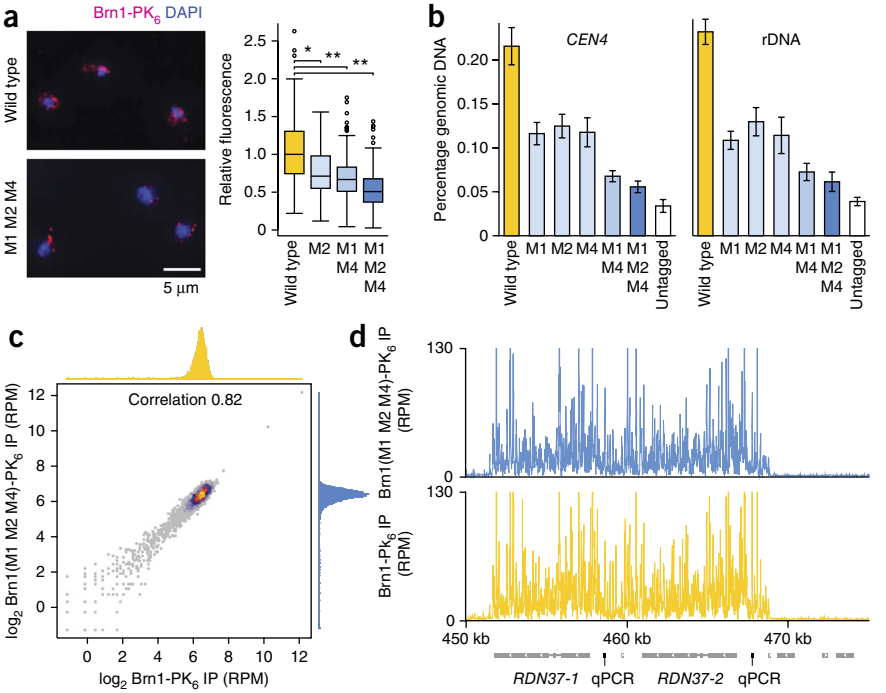

Figure 6 The Ycg1 subunit is essential for condensin recruitment onto yeast chromosomes. (**a**) Chromosome spreads prepared from asynchronous diploid yeast cells (C3632, C3651, C3856 and C3857), probed with anti-PK antibody (red) and stained with 4′,6-diamidino-2-phenylindole (DAPI; blue). Brn1-PK_6 signals were quantified. In box plot at right, horizontal lines define the median, boxes define the 25th and 75th percentiles, and whiskers define the 10th and 90th percentiles. $*P = 8.1 \times 10^{-10}$; $**P < 2.2 \times 10^{-16}$ by one-sided Wilcoxon-Mann-Whitney test. $n = 201$ (wild type), 211 (M2), 243 (M1 M4) or 217 (M1 M2 M4) nuclei from two independent experiments.(**b**) ChIP-qPCR in asynchronous cells of diploid strains expressing wild-type (C3632), single mutants (C3665, C3651 and C3635) or mutant combinations (C3856 and C3857) of Brn1-PK_6 at the centromere of chromosome IV (*CEN4*) and the rDNA locus (5′ untranslated region of *RDN37-1* and *RDN37-2*). Data represent mean values of $n = 4$ ChIP experiments and two technical replicates per experiment ± s.d. (**c**) Scatter plot representing sequence coverage of ChIP-seq reads from yeast expressing wild-type Brn1-PK_6 (strain C3632, *x* axis) and the Brn1 (M1 M2 M4)-PK_6 mutant (strain C3857, *y* axis). Each point represents a 1,000-bp window; the nonparametric Spearman correlation index is indicated. (**d**) Sequence reads (reads per million, RPM) of wild-type and mutant Brn1-PK_6 cells from **c** at the rDNA locus on chromosome XII, displayed on a linear scale. The region used for qPCR analysis in **b** is indicated. In **c** and **d**, sequence reads were normalized to the total number of reads for each sample individually to measure Brn1 positions independent of the absolute efficiency of Brn1 immunoprecipitation.

Recruitment to chromosomes by the HEAT-repeat subunits

To test whether the presence of both HEAT-repeat subunits in condensin complexes is required for condensin's association with chromosomes, we first measured the protein levels associated with mitotic chromosome spreads of wild-type and mutant versions of Brn1 that either reduced (mutant M2) or abolished (M1 M4 double or M1 M2 M4 triple mutants) binding to Ycg1. The amounts of condensin on chromosomes were markedly reduced in all three mutants (**Fig. 6a**). Chromatin immunoprecipitation and quantitative PCR (ChIP-qPCR) at two different chromosomal binding sites confirmed a substantial decrease in condensin association in single, double or triple Brn1 mutants (**Fig. 6b**). To distinguish whether the decrease of condensin levels at these sites was due to the repositioning of condensin to other chromosomal locations or due to a global reduction in chromosome association, we mapped the genome-wide positions of the Brn1 triple mutant by ChIP-seq and compared them to the positions of wild-type Brn1. Our analyses detected no obvious differences between the distributions of wild-type and mutant Brn1 (**Fig. 6c**,**d** and **Supplementary Fig. 7**). These findings do not suggest a role of the HEAT-repeat subunits in targeting to specific chromosome sites but instead suggest that the HEAT-repeat subunits have a crucial function in the general recruitment of condensin onto chromosomes.

To test whether this function is conserved in mammalian condensin complexes, we expressed in human embryonic kidney (HEK) 293 cells wild-type or M1 single, M2 M4 double or M1 M2 M4 triple mutants of the CAP-H kleisin subunit of condensin I or the CAP-H2 kleisin subunit of condensin II (**Fig. 5a** and **Supplementary Fig. 8**). We then immunoprecipitated CAP-H or CAP-H2 via their N-terminal Flag tags and probed for copurification of the other four condensin subunits. Remarkably, the amounts of the Ycg1 homologs CAP-G or CAP-G2 that coimmunoprecipitated with all three CAP-H mutants or the double and triple CAP-H2 mutants, respectively, were greatly reduced (**Fig. 7a** and **Supplementary Fig. 8**). Notably, none of the mutations affected copurification of the other three condensin subunits. We then expressed, at levels below that of the endogenous protein, wild-type and mutant versions of CAP-H fused to enhanced GFP (EGFP) in a HeLa cell line that also expresses histone H2B tagged with mCherry[34] and measured the amounts of CAP-H associated with mitotic chromosomes in cells arrested with nocodazole (**Fig. 7b**). Condensin I enrichment on chromosomes, which we define by the mean EGFP signal ratio of chromosomal to cytoplasmic regions, decreased from ~2.2 in cells expressing wild-type CAP-H to ~1.2–1.4 in cells expressing the CAP-H mutant versions (**Fig. 7c**; a value of 1.0 corresponds to no condensin enrichment on chromosomes). Similarly, condensin II enrichment on chromosomes decreased substantially in the CAP-H2 double and triple mutants but less so in the CAP-H2 single mutant that did not notably affect CAP-G2 binding (**Supplementary Fig. 8**). We conclude that the HEAT-repeat subunits have an essential and conserved role for the recruitment of condensin complexes onto chromosomes in yeast and human cells.

DNA binding by the non-SMC complex stimulates the SMC ATPase

Loading of the condensin-related cohesin complex onto chromosomes depends on ATP hydrolysis by its Smc1–Smc3 subunits, which has been suggested to initiate transport of chromatin fibers into cohesin rings[35,36]. If condensin used a similar mechanism for chromosome loading, we reasoned that DNA binding by the HEAT-repeat subunits might function as a trigger to activate the Smc2–Smc4 ATPase. We found that, consistently with previous reports[13], the presence of DNA had no apparent effect on the low ATPase activity of the

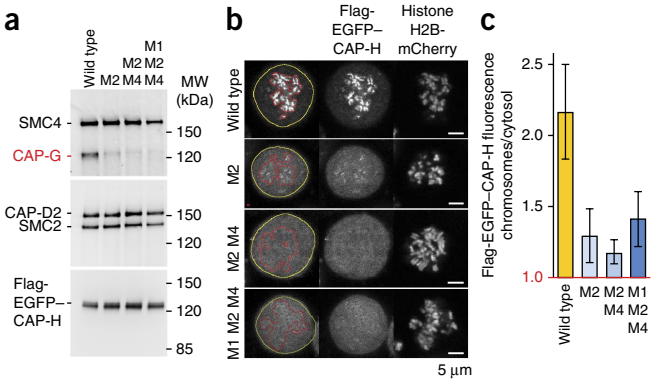

Figure 7 The CAP-G HEAT-repeat subunit is required for condensin binding to human chromosomes. (**a**) Western blotting of coprecipitated condensin subunits. The indicated Flag-EGFP–CAP-H proteins were immunoprecipitated from lysates of transiently transfected HEK293 cells. One representative experiment of $n = 2$ independent experiments is shown. (**b**) Mean EGFP intensities measured in chromosome and cytoplasmic regions. Samples are Flag-EGFP–CAP-H proteins transiently expressed in nocodazole-arrested HeLa cells expressing histone H2B-mCherry. Cells (yellow lines) and chromosomes (red lines) are delineated according to total EGFP or mCherry signals, respectively, and mean EGFP intensities were measured in chromosome and cytoplasmic regions. (**c**) Ratios between chromosomal and cytoplasmic EGFP mean intensities, calculated from one representative experiment of three biological replicates and plotted as mean ± s.d. $n = 92$ (wild type), 59 (M2), 39 (M2 M4) or 76 (M1 M2 M4) cells.

Smc2–Smc4 dimer (~0.5 molecules ATP hydrolyzed per Smc2–Smc4 per minute; **Fig. 8a**,**b**). Addition of the Brn1–Ycs4–Ycg1 non-SMC subcomplex approximately doubled the Smc2–Smc4 ATPase activity in the absence of DNA. Remarkably, simultaneous addition of the Brn1–Ycs4–Ycg1 subcomplex and DNA enhanced the Smc2–Smc4 ATPase activity more than ten-fold (**Fig. 8b**). The DNA-dependent stimulation of the Smc2–Smc4 ATPase activity must have been due to the binding of the non-SMC subcomplex to the Smc2–Smc4 head domains, because we observed no stimulation by DNA when we used a non-SMC subcomplex containing a version of Brn1 that lacks the Smc2–Smc4 interaction motifs (Brn1$_{\Delta NC}$). To rule out that the increase in activity was due to the presence of a contaminating ATPase, we repeated the assay with an Smc2–Smc4 dimer that contained point mutations in each of the two Walker B ATP-hydrolysis motifs. As expected, we measured no DNA-dependent ATPase activity for the mutant Smc2–Smc4 dimer, even in the presence of the non-SMC subcomplex (**Fig. 8b**). Our findings are in full agreement with the report that the ATPase activity of the *Xenopus* condensin holocomplex is higher than that of the SMC2–SMC4 subcomplex and increases in the presence of DNA[12].

DISCUSSION

A DNA-binding site formed by the HEAT-repeat subunits

How condensin complexes interact with their chromatin substrates has remained poorly understood. The Smc2–Smc4 dimer has been previously reported to bind DNA, although binding was considerably less pronounced compared to that of condensin holocomplexes[12] and was disrupted even by medium salt concentrations[13]. Interaction with DNA was proposed to be mediated by the Smc2–Smc4 hinge domains, which, however, bound much more efficiently to ssDNA than to dsDNA[25] and might therefore perform specialized functions of condensin, for example during processes that generate unpaired DNA strands, such as DNA-damage repair or transcription[38]. In previous studies, no DNA binding could be detected for frog or fission-yeast non-SMC subcomplexes[12,15].

We found that the budding-yeast non-SMC subcomplex, in contrast, binds to dsDNA with high selectivity over ssDNA (**Fig. 2a** and **Supplementary Fig. 3**). Our finding that binding to different dsDNA substrates occurred with low micromolar affinity, was reversible and depended on a minimum DNA length (**Fig. 1** and **Supplementary Fig. 2**) does not support the possibility of mere nonspecific electrostatic interactions. These would also seem unlikely for a protein complex with a predicted negative surface charge ($pI = 4.9$). Furthermore, the non-SMC subcomplex from an evolutionarily distant yeast species displayed very similar DNA binding properties (**Fig. 3b**). Because neither the HTH nor the WHD motifs of the kleisin subunit were required for DNA binding

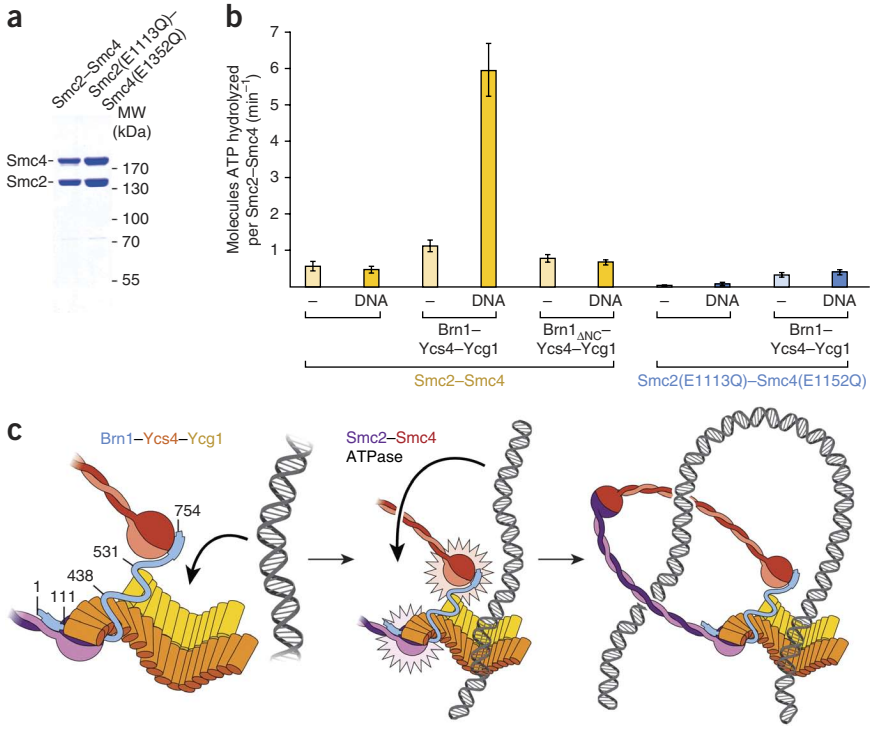

Figure 8 DNA binding by the non-SMC subcomplex activates the Smc2–Smc4 ATPases. (**a**) Wild-type and Walker B–mutant Smc2–Smc4 complexes, analyzed by SDS-PAGE and Coomassie staining. (**b**) Hydrolysis rates of ATP (1.25 mM) in *S. cerevisiae* wild-type or hydrolysis-defective Smc2–Smc4 dimers (0.5 µM), measured in the presence or absence of the Brn1–Ycs4–Ycg1 subcomplex (1.5 µM), the Brn1$_{\Delta NC}$–Ycs4–Ycg1 subcomplex (1.5 µM) lacking the Smc2–Smc4 interaction motifs and/or 6.5-kb linearized plasmid DNA (10 nM). Columns and error bars indicate mean and s.d., respectively, of $n = 3$ technical replicates. (**c**) Multistep model for the topological loading of condensin onto chromosomes. Binding of duplex DNA to the HEAT-repeat subunits (left) activates of the Smc2–Smc4 ATPase activity (middle) to trigger the transfer of DNA into the condensin ring (right). Numbers indicate the binding regions for Ycs4 and Ycg1 in the *S. cerevisiae* Brn1 kleisin subunit.

(**Fig. 1e**,**f**), we suggest that the non-SMC subcomplex binds DNA via its HEAT-repeat subunits. Support for the notion that HEAT repeats can serve as DNA-binding motifs comes from a recent crystal structure of the AlkD glycosylase, which revealed the binding of six HEAT repeats to the phosphate backbone of a 12-bp DNA helix[39] with similar affinities to those that we measured for the interaction of the condensin non-SMC subcomplex with short dsDNA substrates (**Fig. 1d**).

In addition to binding to DNA, condensin holocomplexes have been reported to associate with nucleosomes[12], either via the binding of a phosphorylated N-terminal extension of the γ-kleisin subunits to histones H2A or H2A.Z[18] or via binding of the HEAT-repeat subunits to methylated histone H4 tails[19]. In contrast, we could not detect evidence for an interaction between the non-SMC subcomplex and nucleosomes *in vitro* (**Fig. 2b**) or for the colocalization of condensin with nucleosomes on chromosomes *in vivo* (**Fig. 2c–e** and **Supplementary Fig. 3**). This is consistent with the lack of the N-terminal extension in the γ-kleisin subunits of many yeast species, including *S. cerevisiae*. It is therefore unlikely that the interaction with nucleosomes serves as the universal basis for targeting condensin to chromosomes. We propose that the newly discovered DNA-binding domain fulfills this function instead.

Geometry of the non-SMC subcomplex

Cross-linking MS and copurification analyses showed that the two HEAT-repeat subunits bind to distinct regions of the central domain of the budding-yeast kleisin subunit. A short region within this domain, which contains two conserved patches of hydrophobic residues, is necessary (**Figs. 5b** and **7a** and **Supplementary Fig. 8**) and sufficient (**Fig. 4**) for mediating the interaction with the Ycg1-type HEAT-repeat subunit. This is consistent with the finding that the temperature-sensitive phenotype of the *brn1-60* mutant, which is caused by mutations within patch 1, can be rescued by Ycg1 overexpression[40]. The kleisin region that is required for stable binding to the Ycs4-type HEAT-repeat subunit is, in contrast, considerably larger (**Fig. 4**).

Linkage of the HEAT-repeat subunits by the kleisin notably increased DNA binding (**Fig. 3b**). This enhancement could be due to conformational changes and/or the formation of a combined DNA-binding pocket when the two HEAT-repeat subunits bind to the kleisin subunit. The cooperative action of both HEAT-repeat subunits is presumably essential for condensin function, because association with chromosomes of yeast or human condensin complexes that contain only one HEAT-repeat subunit is strongly reduced (**Figs. 6** and **7** and **Supplementary Fig. 8**), and mutations in either HEAT-repeat protein reduce the levels of chromosome-associated Smc4 in yeast[32]. Because the kleisin subunits of prokaryotic SMC complexes bind to pairs of WHD subunits that have no resemblance to the eukaryotic HEAT-repeat subunits[21], the role of the latter in recruitment of eukaryotic condensin complexes to chromosomes must have been acquired after their evolutionary divergence from a common precursor SMC complex.

A multistep model for loading condensin onto chromosomes

A central feature of SMC protein complexes is the entrapment of chromosomal DNA within their large ring structures[16,41]. How chromatin fibers end up within these protein rings is, however, not understood. For cohesin, it has been suggested that ATP hydrolysis by the Smc1–Smc3 head domains drives the temporary opening of the ring[35,36], presumably at the Smc1–Smc3 hinge interface[42], to allow the entry of chromosomes. Whether condensin might use a similar mechanism is not known. The observation that Smc2 proteins that are defective in ATP hydrolysis can still associate with mitotic chromosomes[43] does not support this possibility. Yet the identification of a direct DNA-binding site in the condensin non-SMC subcomplex explains how condensin can still bind to chromosomes even without encircling them in an ATP hydrolysis–dependent manner. A direct protein-DNA interaction could also be the reason for the requirement of high salt conditions to efficiently release condensin (but not cohesin) from linearized minichromosomes *in vitro*[16].

Our data suggest that binding to DNA via the HEAT-repeat subunits serves as the first step in the condensin-loading mechanism. This interaction consequently activates the Smc2–Smc4 ATPases (**Fig. 8b**). We hypothesize that activation of the ATPase cycle, in a second step, triggers the topological loading of condensin rings onto the tethered chromatin fiber, potentially by inducing a temporary opening of the ring for the passage of DNA (**Fig. 8c**). For cohesin complexes, the role of the HEAT-repeat subunits in the tethering step might have been taken over by a separate Scc2–Scc4 protein complex. Interestingly, Scc2 and Scc4 also contain α-helical repeats and were recently shown to stimulate cohesin's ATPase activity for efficient chromosome loading *in vitro*[44]. How the HEAT-repeat subunits precisely contact DNA, how this leads to activation of the SMC ATPases and how these steps are regulated by post-translational modifications are important questions for future research.

METHODS

Methods and any associated references are available in the online version of the paper.

Accession codes. ChIP-seq data have been deposited in the Gene Expression Omnibus database under accession number GSE55948.

Note: Any Supplementary Information and Source Data files are available in the online version of the paper.

ACKNOWLEDGMENTS

We are grateful to M. Cohen, V. Rybin, M. Saravanan and C. Tischer for assistance with yeast experiments, biophysical assays, nucleosome preparation and image segmentation, to Y. Frosi for suggesting the mutant analysis in human cells and to S. Amlacher and E. Hurt (University of Heidelberg) for providing *C. thermophilum* cDNA and condensin sequences. We thank I. Berger for extensive advice and training in the MultiBac technology and the EMBL Advanced Light Microscopy, Genomics and Proteomics Core Facilities for technical support. We thank V. Benes and B. Baying for discussion, technical advice and help with the preparation of genomic libraries and sequencing. We thank F. Baudin, J. Ellenberg, D. Gilmour, F. Melchior, S. Milles, A. Musacchio, C. Müller and members of the Haering laboratory for discussion and advice. This work was supported by funding from the EMBL and the German Research Foundation (DFG) grant HA 5853/2-1 (C.H.H.). A.O. was supported by postdoctoral fellowships from the Alexander von Humboldt foundation and Marie Curie Actions.

AUTHOR CONTRIBUTIONS

I.P., A.R., A.O., M.W., J.M. and C.H.H. designed and performed the experiments; I.P., A.O. and M.B. analyzed the cross-linking MS experiments; I.P. and V.P. performed bioinformatics analysis of generated and published ChIP-seq data; and I.P. and C.H.H. conceived the project and wrote the manuscript with contributions from all authors.

COMPETING FINANCIAL INTERESTS

The authors declare no competing financial interests.

1. Hirano, T. Condensins: universal organizers of chromosomes with diverse functions. *Genes Dev.* **26**, 1659–1678 (2012).
2. Piazza, I., Haering, C.H. & Rutkowska, A. Condensin: crafting the chromosome landscape. *Chromosoma* **122**, 175–190 (2013).
3. Aragón, L., Martinez-Perez, E. & Merkenschlager, M. Condensin, cohesin and the control of chromatin states. *Curr. Opin. Genet. Dev.* **23**, 204–211 (2013).

4. Wood, A.J., Severson, A.F. & Meyer, B.J. Condensin and cohesin complexity: the expanding repertoire of functions. *Nat. Rev. Genet.* **11**, 391–404 (2010).
5. Anderson, D.E., Losada, A., Erickson, H.P. & Hirano, T. Condensin and cohesin display different arm conformations with characteristic hinge angles. *J. Cell Biol.* **156**, 419–424 (2002).
6. Schleiffer, A. *et al.* Kleisins: a superfamily of bacterial and eukaryotic SMC protein partners. *Mol. Cell* **11**, 571–575 (2003).
7. Onn, I., Aono, N., Hirano, M. & Hirano, T. Reconstitution and subunit geometry of human condensin complexes. *EMBO J.* **26**, 1024–1034 (2007).
8. Neuwald, A.F. & Hirano, T. HEAT repeats associated with condensins, cohesins, and other complexes involved in chromosome-related functions. *Genome Res.* **10**, 1445–1452 (2000).
9. Ono, T., Fang, Y., Spector, D.L. & Hirano, T. Spatial and temporal regulation of condensins I and II in mitotic chromosome assembly in human cells. *Mol. Biol. Cell* **15**, 3296–3308 (2004).
10. Kimura, K. & Hirano, T. ATP-dependent positive supercoiling of DNA by 13S condensin: a biochemical implication for chromosome condensation. *Cell* **90**, 625–634 (1997).
11. Kimura, K., Rybenkov, V.V., Crisona, N.J., Hirano, T. & Cozzarelli, N.R. 13S condensin actively reconfigures DNA by introducing global positive writhe: implications for chromosome condensation. *Cell* **98**, 239–248 (1999).
12. Kimura, K. & Hirano, T. Dual roles of the 11S regulatory subcomplex in condensin functions. *Proc. Natl. Acad. Sci. USA* **97**, 11972–11977 (2000).
13. Stray, J.E. & Lindsley, J.E. Biochemical analysis of the yeast condensin Smc2/4 complex: an ATPase that promotes knotting of circular DNA. *J. Biol. Chem.* **278**, 26238–26248 (2003).
14. Stray, J.E., Crisona, N.J., Belotserkovskii, B.P., Lindsley, J.E. & Cozzarelli, N.R. The *Saccharomyces cerevisiae* Smc2/4 condensin compacts DNA into (+) chiral structures without net supercoiling. *J. Biol. Chem.* **280**, 34723–34734 (2005).
15. Sakai, A., Hizume, K., Sutani, T., Takeyasu, K. & Yanagida, M. Condensin but not cohesin SMC heterodimer induces DNA reannealing through protein-protein assembly. *EMBO J.* **22**, 2764–2775 (2003).
16. Cuylen, S., Metz, J. & Haering, C.H. Condensin structures chromosomal DNA through topological links. *Nat. Struct. Mol. Biol.* **18**, 894–901 (2011).
17. Haering, C.H., Farcas, A.-M., Arumugam, P., Metson, J. & Nasmyth, K. The cohesin ring concatenates sister DNA molecules. *Nature* **454**, 297–301 (2008).
18. Tada, K., Susumu, H., Sakuno, T. & Watanabe, Y. Condensin association with histone H2A shapes mitotic chromosomes. *Nature* **474**, 477–483 (2011).
19. Liu, W. *et al.* PHF8 mediates histone H4 lysine 20 demethylation events involved in cell cycle progression. *Nature* **466**, 508–512 (2010).
20. Gajiwala, K.S. & Burley, S.K. Winged helix proteins. *Curr. Opin. Struct. Biol.* **10**, 110–116 (2000).
21. Bürmann, F. *et al.* An asymmetric SMC–kleisin bridge in prokaryotic condensin. *Nat. Struct. Mol. Biol.* **20**, 371–379 (2013).
22. Haering, C.H. *et al.* Structure and stability of cohesin's Smc1-kleisin interaction. *Mol. Cell* **15**, 951–964 (2004).
23. Woo, J.-S. *et al.* Structural studies of a bacterial condensin complex reveal ATP-dependent disruption of intersubunit interactions. *Cell* **136**, 85–96 (2009).
24. Yoshimura, S.H. *et al.* Condensin architecture and interaction with DNA: regulatory non-SMC subunits bind to the head of SMC heterodimer. *Curr. Biol.* **12**, 508–513 (2002).
25. Griese, J.J., Witte, G. & Hopfner, K.-P. Structure and DNA binding activity of the mouse condensin hinge domain highlight common and diverse features of SMC proteins. *Nucleic Acids Res.* **38**, 3454–3465 (2010).
26. Lowary, P.T. & Widom, J. New DNA sequence rules for high affinity binding to histone octamer and sequence-directed nucleosome positioning. *J. Mol. Biol.* **276**, 19–42 (1998).
27. Mavrich, T.N. *et al.* A barrier nucleosome model for statistical positioning of nucleosomes throughout the yeast genome. *Genome Res.* **18**, 1073–1083 (2008).
28. Albert, I. *et al.* Translational and rotational settings of H2A.Z nucleosomes across the *Saccharomyces cerevisiae* genome. *Nature* **446**, 572–576 (2007).
29. Amlacher, S. *et al.* Insight into structure and assembly of the nuclear pore complex by utilizing the genome of a eukaryotic thermophile. *Cell* **146**, 277–289 (2011).
30. Leitner, A. *et al.* Probing native protein structures by chemical cross-linking, mass spectrometry, and bioinformatics. *Mol. Cell. Proteomics* **9**, 1634–1649 (2010).
31. Leitner, A. *et al.* Expanding the chemical cross-linking toolbox by the use of multiple proteases and enrichment by size exclusion chromatography. *Mol. Cell Proteomics* **11**, M111.014126 (2012).
32. Lavoie, B.D., Hogan, E. & Koshland, D. *In vivo* dissection of the chromosome condensation machinery: reversibility of condensation distinguishes contributions of condensin and cohesin. *J. Cell Biol.* **156**, 805–815 (2002).
33. Cuylen, S., Metz, J., Hruby, A. & Haering, C.H. Entrapment of chromosomes by condensin rings prevents their breakage during cytokinesis. *Dev. Cell* **27**, 469–478 (2013).
34. Neumann, B. *et al.* Phenotypic profiling of the human genome by time-lapse microscopy reveals cell division genes. *Nature* **464**, 721–727 (2010).
35. Arumugam, P. *et al.* ATP hydrolysis is required for cohesin's association with chromosomes. *Curr. Biol.* **13**, 1941–1953 (2003).
36. Weitzer, S., Lehane, C. & Uhlmann, F. A model for ATP hydrolysis-dependent binding of cohesin to DNA. *Curr. Biol.* **13**, 1930–1940 (2003).
37. Arumugam, P., Nishino, T., Haering, C.H., Gruber, S. & Nasmyth, K. Cohesin's ATPase activity is stimulated by the C-terminal winged-helix domain of its kleisin subunit. *Curr. Biol.* **16**, 1998–2008 (2006).
38. Akai, Y. *et al.* Opposing role of condensin hinge against replication protein A in mitosis and interphase through promoting DNA annealing. *Open Biol.* **1**, 110023 (2011).
39. Rubinson, E.H., Gowda, A.S.P., Spratt, T.E., Gold, B. & Eichman, B.F. An unprecedented nucleic acid capture mechanism for excision of DNA damage. *Nature* **468**, 406–411 (2010).
40. Ouspenski, I.I., Cabello, O.A. & Brinkley, B.R. Chromosome condensation factor Brn1p is required for chromatid separation in mitosis. *Mol. Biol. Cell* **11**, 1305–1313 (2000).
41. Ivanov, D. & Nasmyth, K. A topological interaction between cohesin rings and a circular minichromosome. *Cell* **122**, 849–860 (2005).
42. Gruber, S. *et al.* Evidence that loading of cohesin onto chromosomes involves opening of its SMC hinge. *Cell* **127**, 523–537 (2006).
43. Hudson, D.F. *et al.* Molecular and genetic analysis of condensin function in vertebrate cells. *Mol. Biol. Cell* **19**, 3070–3079 (2008).
44. Murayama, Y. & Uhlmann, F. Biochemical reconstitution of topological DNA binding by the cohesin ring. *Nature* **505**, 367–371 (2014).

ONLINE METHODS

Protein expression and purification. Non-SMC subunits and subcomplexes (**Supplementary Table 1**) were cloned into a single bacmid according to the MultiBac protocol[45]. Owing to ambiguities of the start-codon annotation, the N-terminal 26 residues of *Ct*Ycg1 and *Ct*Ycs4 were removed. The C-terminal tail of *Ct*Ycg1 was removed because it was predicted to be unstructured. Proteins were coexpressed in Sf21 cells cultured in Sf-900 III SFM serum-free medium (Invitrogen). About 2×10^9 Sf21 cells were lysed with a tissue grinder in lysis buffer (25 mM Tris-HCl, pH 8.0, 250 mM NaCl, 10 mM imidazole, and 0.1% NP-40) containing 50 µM leupeptin (Serva), 5 µM pepstatin (Serva), 1× Pefabloc SC (Serva), 30 µg/µL DNase I (Roche), and 5 mM β-mercaptoethanol at 4 °C. After centrifugation at 45,000*g* for 30 min at 4 °C, cleared lysates were loaded onto Ni-NTA Fast Flow (GE Healthcare) and/or Strep-Tactin Superflow (IBA) columns. Columns were washed extensively with wash buffer (25 mM Tris-HCl, pH 8.0, 150–300 mM NaCl, and 5 mM β-mercaptoethanol, plus 30 mM imidazole for Ni-NTA). Proteins were eluted with five column volumes (CVs) of elution buffer (25 mM Tris-HCl, pH 8.0, and 150 mM NaCl, plus 300 mM imidazole for Ni-NTA or 3 mM D-desthiobiotin for Strep-Tactin). Eluates were loaded onto a Source 15Q 4.6/100 PE anion-exchange column (GE Healthcare) preequilibrated with 20 mM HEPES-KOH, pH 8.0, 150 mM NaCl, and 0.4 mM TCEP. The column was washed with 10 CVs of the same buffer and eluted by increasing the NaCl concentration to 1 M in a gradient of 25 ml. Peak fractions were concentrated by ultrafiltration (Vivaspin 100,000 MWCO, Sartorius) and loaded onto a Superose 6 size-exclusion column (GE Healthcare) in 20 mM HEPES-KOH, pH 8.0, 180 mM NaCl, 2% glycerol, and 0.4 mM TCEP.

Recombinant nucleosomes were reconstituted by salt dialysis as described[46,47], with *S. cerevisiae* recombinant histone octamers and a 167-bp dsDNA fragment derived from the strong 601 positioning sequence[26].

Genes encoding the *S. cerevisiae* Smc2 and Smc4-His_6 hinge domains were cloned in the pET28 *Escherichia coli* expression vector. Expression was induced for 16 h at 18 °C in the *E. coli* BL21-CodonPlus(DE3)-RIPL strain (Agilent) and purified after lysis by sonication via Ni-NTA as described above. Eluate fractions were dialyzed against 20 mM sodium phosphate (NaP_i), pH 7.2, 300 mM NaCl, and 2 mM DTT and loaded onto a Superdex 200 26/60 gel-filtration column (GE Healthcare) equilibrated in 20 mM NaP_i, pH 7.2, 1 mM EDTA, 300 mM NaCl, 1 mM NaN_3, and 2 mM DTT.

Smc2-His_6 and Smc4-StrepII were coexpressed from the pGAL10 or pGAL1 promoter, respectively, on a 2µ-based plasmid in *S. cerevisiae*. Yeast cells were grown at 30 °C in tryptophan-dropout medium containing 2% raffinose to early log phase, and expression was induced for 12 h by addition of galactose to 2%. Cells were harvested and resuspended in lysis buffer (50 mM Tris-HCl, pH 7.5, 200 mM NaCl, 2× Complete EDTA-free protease-inhibitor mix (Roche)), and broken by cryogenic lysis in a Freezer/Mill (Spex). Extracts were cleared by centrifugation at 43,400*g* and loaded onto 6 ml of Ni-NTA Fast Flow after imidazole was adjusted to 20 mM. Proteins were eluted in lysis buffer plus 300 mM imidazole and loaded onto 5 ml of Strep-Tactin Superflow high capacity after addition of EDTA and DTT to 1 mM. Proteins were eluted in lysis buffer plus 10 mM desthiobiotin and loaded onto a Superose 6 size-exclusion column in 20 mM Tris-HCl, pH 7.5, 150 mM NaCl, and 1 mM DTT. Wild-type and mutant Smc2–Smc4 dimers were concentrated to 1–3 mg/ml by ultrafiltration (Vivaspin 30,000 MWCO).

Electron microscopy. Protein samples were diluted to 0.02 µg/µl and applied onto custom-made carbon-coated grids glow-discharged in air. Grids were stained with 2% uranyl acetate and air dried for 10 min before imaging in a Morgagni FEI TEM operated at 100 kV and equipped with an SIS MegaView CCD camera at 40,000× magnification.

DNA binding assays. Linear 6.5-kb dsDNA templates were prepared by SpeI digestion of a circular plasmid containing part of the rDNA repeat sequence[16]. 15- to 60-bp dsDNA substrates were generated by annealing complementary HPLC-purified oligonucleotides (IDT), one of which was labeled with 6-FAM at the 5′ end (**Supplementary Fig. 2b**), at a final concentration of 20 µM in 10 mM HEPES-KOH, pH 7.5, 125 mM NaCl, and 5 mM $MgCl_2$. Successful annealing and purity of the oligonucleotides were confirmed by electrophoresis and size-exclusion chromatography.

Reaction mixtures for the EMSA experiments contained a final concentration of 9.5 pM of 6.5-kb dsDNA or 200 nM of DNA oligos and varying concentrations of non-SMC or Smc2–Smc4 hinge complexes in 50 mM HEPES-KOH, pH 7.5, 650 mM NaCl, 35 mM $MgCl_2$ and 5 mM β-mercaptoethanol in a volume of 50 µl. To test binding to recombinant nucleosomes, 4 µg histone octamers were dialyzed against 50 mM HEPES-KOH, pH 7.5, 650 mM NaCl, 35 mM $MgCl_2$, 5 mM β-mercaptoethanol and an equimolar amount of 167-bp DNA. The resulting nucleosomes were incubated with varying concentrations of non-SMC complex in the same buffer conditions. DNA–protein complexes were resolved by electrophoresis at 4 °C on 0.7% TAE-agarose gels (16 h at 3 V/cm) for the 6.5-kb dsDNA substrate, on 1.8% TBE-agarose gels (5 h at 8 V/cm) for 15- to 60-bp dsDNA and 30-bp ssDNA substrates, or on 1.6% TBE-agarose gels (overnight at 3 V/cm) for Nuc-167. Nuc-167 and 6.5-kb dsDNA were detected by ethidium bromide staining, and 6-FAM–labeled oligonucleotides were visualized at $\lambda_{em} = 520$ nm with an FLA-7000 scanner (Fujifilm).

Fluorescence anisotropy experiments were carried out at 100 nM 6-FAM DNA and variable concentrations of protein (0.006–36 µM). Anisotropy readings were recorded after 30-min incubation of the binding reactions at room temperature in a microplate reader (BioTek) at $\lambda_{ex} = 485$ nm and $\lambda_{em} = 525$ nm.

Normalized fluorescence anisotropy (ΔA) was calculated using

$$\Delta A = (r_n - r_0)/(r_{max} - r_0)$$

where r_0 is the anisotropy without protein, and r_{max} is the anisotropy at the highest protein concentration. For estimating equilibrium dissociation constants (K_d), the normalized fluorescence anisotropy was plotted as a function of protein concentration, and a curve was fit to the full quadratic expansion of the binding polynomial derived for the total concentrations of:

$$\Delta A = \frac{\Delta A_T}{2D_T}\left\{\left(E_T + D_T + Kd\right) - \sqrt{\left(E_T + D_T + Kd\right)^2 - 4E_T D_T}\right\}$$

where ΔA_T is the total anisotropy change after saturation of the curve, E_T is the total protein concentration at each point in the titration, and D_T is the total DNA concentration. The DNA-protein binding constants were confirmed in two independent experiments performed with different batches of purified proteins.

Subunit mapping by cross-linking mass spectrometry. 0.1–5 mM H^{12}-D^{12} isotope-labeled in disuccinimidyl suberate (Creative Molecules) was mixed with 50 µg of the non-SMC complex in 20 mM HEPES-KOH, pH 8.0, 200 mM NaCl, and 0.5 mM TCEP. Cross-linking reactions were incubated for 40 min at 24 °C and quenched by addition of NH_4HCO_3 to 0.1 M for 10 min at 24 °C. Cross-linked proteins were denatured in 4 M urea and 0.1% RapiGest (Waters) and then treated with 10 mM DTT for 30 min at 37 °C, and with 15 mM iodoacetamide for 30 min in the dark. After dilution of the urea concentration to 1.5 M, protein was digested first with 0.5 µg Lys-C endoproteinase (Wako) for 4 h at 37 °C and then with 1 µg trypsin (Promega) overnight at 37 °C. Trifluoroacetic acid (TFA) was added to 0.5% (v/v). Peptides were desalted with MicroSpin columns (Harvard Apparatus), dried, and reconstituted with 30% (v/v) acetonitrile in 0.1% (v/v) formic acid. Cross-linked peptides were enriched by size-exclusion chromatography on a Superdex Peptide PC 3.2/30 column (GE Healthcare) as described[31].

Between 2% and 10% of the size-exclusion fractions were loaded onto a BEH300 C18 (75 µm × 250 mm, 1.7 µm) nanoAcquity UPLC column (Waters) connected online to an LTQ-Orbitrap Velos Pro mass spectrometer (Thermo), and were eluted stepwise with a gradient of 3–85% (v/v) ACN in 0.1% (v/v) formic acid. Data acquisition was performed with a TOP-20 strategy in which survey MS scans (m/z range 375–1,600) were acquired in the Orbitrap ($R = 30{,}000$), and up to 20 of the most abundant ions per full scan were fragmented by collision-induced dissociation (normalized collision energy = 40, activation $Q = 0.250$) and analyzed in the LTQ. In order to focus the acquisition on larger cross-linked peptides, charge states 1, 2, and unknown were rejected. Dynamic exclusion was enabled with repeat count = 1, exclusion duration = 60 s, list size = 500, and mass window ± 15 p.p.m. Ion target values were 1,000,000 (or 500-ms maximum fill time) for full scans and 10,000 (or 50-ms maximum fill time) for MS/MS scans. At least two technical replicates per sample were measured.

Raw files were converted to centroid mzXML with the MassMatrix file-conversion tool[48] and then analyzed with xQuest[49] and xProphet[50]. The results

were filtered with the following parameters: FDR = 0.05; minimum delta score = 0.95; MS1 tolerance window ± 3 p.p.m. All selected cross-links were classified, and only high-confidence linkages with an LD score >20 (**Supplementary Fig. 5b**) observed in at least two independent experiments were considered.

Multisequence alignments. Sequence alignments were performed with T-Coffee[51], and secondary-structure predictions were obtained from the Phyre2 protein homolog- and fold-recognition server[52]. Conserved residues were highlighted accordingly to the ClustalW color code[32,33,53].

Yeast experiments. All strains are derivatives of W303; detailed genotypes are listed in **Supplementary Table 5**. Segregation of chromosome V was monitored by FACScan and live-cell microscopy as described[16].

Input, unbound, and bound samples (10×) from yeast immunoprecipitation experiments were separated on 4–12% or 7% SDS-PAGE and probed by western blotting against Protein A (1:5,000, Sigma, cat. no. P1291), HA (1:15,000, Abcam, cat. no. ab9110), myc (1:10,000, Gramsch, cat. no. CM-100), PK (1:1,000, AbD Serotec, cat. no. MCA1360), or *S. cerevisiae* Ycg1 residues 1–524 (polyclonal antibody raised in rabbit, 1:1,000, Eurogentec). Validation of commercial antibodies is available on the manufacturers' websites.

Condensin and purification from yeast extracts. Expression of truncated versions of Brn1 fused to a Protein A tag was induced from an ectopic copy of the gene under the control of the galactose-inducible *GAL10* promoter on a centromeric plasmid by addition to the medium of galactose to 2% for 4 h at 30 °C. Extracts from ~50 mOD_{600} culture were prepared by glass-bead lysis in 1 ml EBX buffer (50 mM HEPES-KOH, pH 7.5, 100 mM KCl, 2.5 mM $MgCl_2$, 0.25% Triton X-100, and 1 mM DTT) plus 2× Complete, EDTA-free protease-inhibitor mix (Roche) and 1 mM PMSF and cleared by 15 min centrifugation at 19,000*g*. Brn1–Protein A fusion proteins were purified by addition of 25 µl (bed volume) IgG Sepharose FF (GE Healthcare) for 2 h at 4 °C. This was followed by three 10-min wash steps in EBX (low salt) or one 10-min wash step in EBX and two 10-min wash steps in EBX + 200 mM KCl (high salt), and elution by 5-min incubation at 95 °C in 100 µl 1× Laemmli loading buffer.

For the purification of endogenous condensin complexes, 2×10^3 OD_{600} cells were resuspended in 7 ml lysis buffer (50 mM Tris-HCl, pH 8.0, 100 mM NaCl, 2.5 mM $MgCl_2$, 0.15% Triton X-100, and 1 mM DTT) plus 1× Complete, EDTA-free protease-inhibitor mix (Roche) and 1 mM PMSF, snap frozen as pellets in liquid nitrogen, and broken by cryogenic lysis in a Freezer/Mill (Spex). Cell extracts were cleared by 15-min centrifugation at 45,000*g* at 4 °C. Ten µl Anti-V5 tag antibody (AbD Serotec, cat. no. MCA1360) was added for 5 h at 4 °C. This was followed by addition of 50 µl (bed volume) of Protein G Dynabeads (Invitrogen) for 16 h at 4 °C. Dynabeads were washed five times with lysis buffer, and bound proteins were eluted in 25 µl 1× loading buffer.

Chromosome spreads, ChIP-qPCR, and ChIP-seq. Chromosome spreads and ChIP-qPCR were performed as described[16], with the exception that fixation for ChIP-qPCR was performed in 3% (v/v) formaldehyde at room temperature. Primers for the *CEN4* locus were TGGTGTGGAAGTCCTAATATCG and TGCATGATCAAAAGGCTCAA. Primers for the rDNA locus were TTTCTGCCTTTTTCGGTGAC and TGGCATGGATTTCCCTTTAG.

For ChIP-seq analysis of PK_6-tagged Brn1, chromatin from asynchronous yeast cells was digested with 160 U micrococcal nuclease (Worthington Biochemicals) and purified with a MinElute PCR purification kit (Qiagen). Samples combined from three independent experiments were sequenced on a MiSeq Desktop Sequencer (Illumina). Paired-end sequencing reads were mapped to the *S. cerevisiae* genome (http://yeastgenome.org/ version R64-1-1) with Bowtie 2, v2.1.0, with default settings[34,54]. Reads with identical boundaries were discarded as PCR duplicates, and the central position of each paired read mapping uniquely to the genome (mapq > 10) was used for computing the sequencing coverage, except for the data in **Figure 6d** (which displays the region of chromosome XII containing the two annotated rDNA repeats (coordinates 451,000–468,500)), in which reads mapping multiple times to the genome were also used. Library size was normalized to 1 million reads and coverage expressed as reads per million (RPM = number of mapped reads for each chromosomal coordinate point/total number of mapped reads × 10^6). H2A.Z ChIP-seq data (Htz1-TAP) were downloaded from GEO (GSE47073) and processed as described for Brn1-PK_6. Data sets for nucleosome position[27,35,36] and H2A.Z-enriched nucleosome position[28] were downloaded from the *Saccharomyces* Genome Database (http://yeastgenome.org/) to classify subregions of the budding-yeast genome as nucleosome depleted or as nucleosome enriched. To exclude regions with weakly bound or poorly positioned nucleosomes from the analysis, nucleosome-depleted regions were defined as those DNA regions located between adjacent nucleosomes with sizes between 10 and 100 bp. Brn1-PK_6 binding was determined independently for each chromosome, and the statistical analysis to test whether Brn1 binds preferentially to the regions classified as nucleosome enriched or nucleosome depleted was performed with R and Bioconductor (http://www.bioconductor.org/). To infer differential signals between genome-wide binding sites of Brn1-PK_6 and Brn1(M1 M2 M4)-PK_6, the DESeq2 package for R/Bioconductor was used[55].

Purification and chromosome binding of human condensin complexes. Single or multiple point mutations (**Supplementary Table 4**) were introduced into pC1-Flag-EGFP–CAP-H or Flag-EGFP–CAP-H2 (ref. 56) and used to perform transient transfections of Flp-In-293 HEK cells (Life Technologies). Approximately 2×10^6 cells seeded in a 60-mm petri dish were treated with transfection mix (2 µg plasmid DNA, 6 µl Lipofectamine 2000 (Invitrogen), and 100 µl Opti-MEM medium (Life Technologies)) and incubated for 6 h. Opti-MEM medium was then replaced with high-glucose DMEM medium (Life Technologies) supplemented with 10% serum, 1% PenStrep (Invitrogen), and 1% glutamine (Invitrogen). Cells were harvested after 18 h with a cell scraper and resuspended in 300 µl Cell Lytic M buffer (Sigma) supplemented with 2 mM DTT, 2× Complete EDTA-free protease-inhibitor mix (Roche), and 1 mM PMSF. Equivalent amounts of cleared protein extract were incubated for 2 h at 4 °C with 5 µl anti-Flag antibody (monoclonal M2, Sigma, cat. no. F3165) and then overnight with 50 µl Protein G Dynabeads (Invitrogen). Conjugated beads were washed twice with Cell Lytic M buffer supplemented with 2 mM DTT and 1 mM PMSF, and bound proteins were eluted win 60 µl 2× loading buffer. Antibodies used for western blotting against CAP-H (1:2,000, cat. no. A300-603A), CAP-G (1:2,000 cat. no. A300-602A), CAP-D2 (1:2,000, cat. no. A300-601A), CAP-H2 (1:1,000, cat. no. A302-275A), CAP-D3 (1:500, A300-604A), SMC2 (1:5,000, A300-058A) and SMC4 (1:2,000, A300-064A) were obtained from Bethyl Laboratories, and antibody against CAP-G2 was obtained from Abgent (1:500, cat. no. WA-AP17069c.80). Antibody validations can be found online on the manufacturers' websites.

Imaging was performed with HeLa Kyoto H2B-mCherry cells[34]. Cells were seeded into 35-mm dishes (MatTek) and transfected at 50–70% confluency as described above. Fresh medium containing 100 ng/ml nocodazole was added 5–12 h before imaging. Cells were washed once and then imaged in 20 mM HEPES-KOH, pH 7.4, 115 mM NaCl, 1.2 mM $CaCl_2$, 1.2 mM $MgCl_2$, 1.2 mM K_2HPO_4, and 2 g/l D-glucose. Images were acquired at 37 °C on a Zeiss LSM 780 microscope in 16-bit mode with four lines averaging with a Plan-Apochromat 63×/1.40 oil DIC M27 objective. Excitation and emission wavelengths were 488 nm and 520–560 nm for EGFP or 561 nm and 580–650 nm for mCherry. All used cell lines were tested for mycoplasma contamination.

Image analysis. Dual-color images of mitotic cells were analyzed with CellProfiler[57]. Background levels in the EGFP channel were measured outside cells and subtracted globally. Subsequently, a median filter was applied to correct for noise, and fluorescence signals not belonging to the central mitotic cell were automatically removed on the basis of their limited spatial extension with a morphological opening filter. The remaining signal was used to segment the cell by means of a manual threshold. Chromosomes were segmented with a manual threshold on the H2B channel after application of a median filter. Mean intensity signals were then measured in the chromosome regions and in the intracellular region excluding the chromosome regions (i.e., the cytoplasmic region) of background-subtracted but otherwise unfiltered EGFP images.

ATPase assays. ATPase assays were performed as described[37] with 0.5 µM Smc2–Smc4 dimer, with or without 1.5 µM non-SMC subcomplex and/or 10 nM linearized 6.5-kb plasmid DNA, in 20 mM Tris-HCl, pH 7.8, 150 mM NaCl, 12.5 mM $MgCl_2$, and 1.25 mM ATP (plus 33 nM [α-^{32}P]ATP; Hartmann Analytic), and 1 mM DTT. Ten-microliter reactions were incubated at 30 °C, and 1 µl was spotted onto PEI cellulose F TLC plates (Merck) every 5 min for 25 min. TLC plates were developed in 0.5 M LiCl, and 1 M formic acid, exposed to phosphorimager plates

doi:10.1038/nsmb.2831

and analyzed with a Typhoon FLA-7000 scanner. ATP hydrolysis rates were calculated from the ADP/ATP ratios of time points in the linear range of the reaction.

Original images. Original images of gels and blots used in this study can be found in **Supplementary Figure 9**.

45. Fitzgerald, D.J. *et al.* Protein complex expression by using multigene baculoviral vectors. *Nat. Methods* **3**, 1021–1032 (2006).
46. Luger, K., Rechsteiner, T.J. & Richmond, T.J. Preparation of nucleosome core particle from recombinant histones. *Methods Enzymol.* **304**, 3–19 (1999).
47. Saravanan, M. *et al.* Interactions between the nucleosome histone core and Arp8 in the IN080 chromatin remodeling complex. *Proc. Natl. Acad. Sci. USA* **109**, 20883–20888 (2012).
48. Xu, H., Zhang, L. & Freitas, M.A. Identification and characterization of disulfide bonds in proteins and peptides from tandem MS data by use of the MassMatrix MS/MS search engine. *J. Proteome Res.* **7**, 138–144 (2008).
49. Rinner, O. *et al.* Identification of cross-linked peptides from large sequence databases. *Nat. Methods* **5**, 315–318 (2008).
50. Walzthoeni, T. *et al.* False discovery rate estimation for cross-linked peptides identified by mass spectrometry. *Nat. Methods* **9**, 901–903 (2012).
51. Notredame, C., Higgins, D.G. & Heringa, J. T-Coffee: a novel method for fast and accurate multiple sequence alignment. *J. Mol. Biol.* **302**, 205–217 (2000).
52. Kelley, L.A. & Sternberg, M.J.E. Protein structure prediction on the Web: a case study using the Phyre server. *Nat. Protoc.* **4**, 363–371 (2009).
53. Thompson, J.D., Higgins, D.G. & Gibson, T.J. CLUSTAL W: improving the sensitivity of progressive multiple sequence alignment through sequence weighting, position-specific gap penalties and weight matrix choice. *Nucleic Acids Res.* **22**, 4673–4680 (1994).
54. Langmead, B. & Salzberg, S.L. Fast gapped-read alignment with Bowtie 2. *Nat. Methods* **9**, 357–359 (2012).
55. Anders, S. & Huber, W. Differential expression analysis for sequence count data. *Genome Biol.* **11**, R106 (2010).
56. Gerlich, D., Hirota, T., Koch, B., Peters, J.-M. & Ellenberg, J. Condensin I stabilizes chromosomes mechanically through a dynamic interaction in live cells. *Curr. Biol.* **16**, 333–344 (2006).
57. Carpenter, A.E. *et al.* CellProfiler: image analysis software for identifying and quantifying cell phenotypes. *Genome Biol.* **7**, R100 (2006).